Accepted Manuscript

Structural defect accumulation in tungsten and tungsten-5wt.% tantalum under incremental proton damage

I. Ipatova, R.W. Harrison, P.T. Wady, S.M. Shubeita, D. Terentyev, S.E. Donnelly, E. Jimenez-Melero

PII: S0022-3115(17)31030-9

DOI: 10.1016/j.jnucmat.2017.11.030

Reference: NUMA 50639

To appear in: *Journal of Nuclear Materials*

Received Date: 18 July 2017

Revised Date: 2 October 2017

Accepted Date: 18 November 2017

Please cite this article as: I. Ipatova, R.W. Harrison, P.T. Wady, S.M. Shubeita, D. Terentyev, S.E. Donnelly, E. Jimenez-Melero, Structural defect accumulation in tungsten and tungsten-5wt.% tantalum under incremental proton damage, *Journal of Nuclear Materials* (2018), doi: 10.1016/j.jnucmat.2017.11.030.

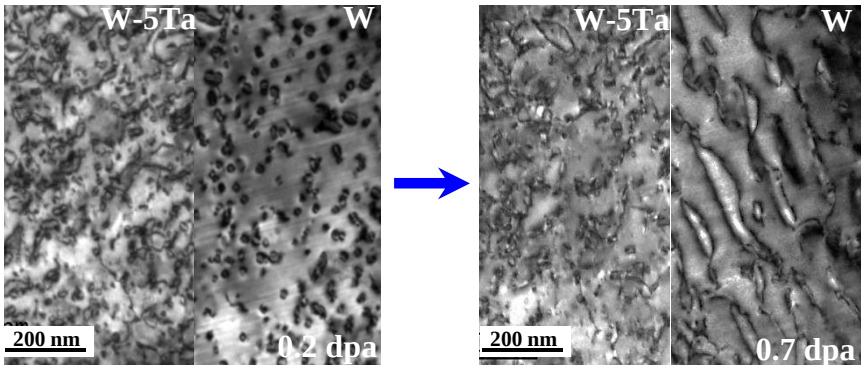

Structural defect accumulation in tungsten and tungsten-5wt.% tantalum under incremental proton damage

I. Ipatova[a,b,*], R.W. Harrison[c], P.T. Wady[b], S.M. Shubeita[b], D. Terentyev[d], S.E. Donnelly[c], E. Jimenez-Melero[a]

[a] *School of Materials, The University of Manchester, Manchester M13 9PL, UK*

[b] *Dalton Cumbrian Facility, The University of Manchester, Moor Row CA24 3HA, UK*

[c] *School of Computing and Engineering, University of Huddersfield, Huddersfield, HD1 3DH, UK*

[d] *SCK·CEN, Nuclear Materials Science Institute, Boeretang 200, Mol, 2400, Belgium*

Corresponding author (*):

University of Manchester

School of Materials

Oxford Road

Manchester

M13 9PL

United Kingdom

Tel.: +44 7849290480

Email: iuliia.ipatova@postgrad.manchester.ac.uk

Abstract

We have performed proton irradiation of W and W-5wt.%Ta materials at 350°C with a step-wise damage level increase up to 0.7 dpa and using two beam energies, namely 40keV and 3MeV, in order to probe the accumulation of radiation-induced lattice damage in these materials. Interstitial-type *a*/2 <111> dislocation loops form under irradiation, and their size increases in W-5Ta up to a loop width of 21(4) nm at 0.3 dpa, where loop saturation takes place. In contrast, the loop length in W increases progressively up to 183(50) nm at 0.7 dpa, whereas the loop width remains relatively constant at 29(7) nm and ≥0.3 dpa, giving rise to dislocation strings. The dislocation loops and networks observed in both materials at later stages act as effective hydrogen trapping sites, so as to generate hydrogen bubbles and surface blisters. Ta doping delays the evolution of radiation-induced dislocation structures in W, and consequently the appearance of hydrogen blisters.

Keywords: refractory metals, dislocation analysis, proton irradiation, transmission electron microscopy, blisters

1. Introduction

Tungsten (W) and its alloys are leading material candidates for plasma-facing components of magnetically-confined fusion reactors, especially in high-heat-flux regions such as the divertor [1-3]. The attractiveness of W-based materials lies in their high resistance to plasma-induced sputtering, erosion and swelling, their thermal conductivity and high-temperature strength [4-7]. These materials will be exposed during service to high-heat loads between 0.1 and 20 MW/m^2 [8, 9]. During plasma disruptions and edge-localised mode events, heat loads can even reach up to the GW/m^2 range [10]. Unfortunately, the ductile-to-brittle transition temperature (DBTT) of tungsten is relatively high, namely 200–400°C depending on its processing route and resultant grain structure [11, 12]. The DBTT is also reported to increase with neutron irradiation up to ~800–1000°C [13, 14]. The brittle nature of tungsten can lead to premature failure during low-temperature reactor operations [15]. Moreover, the neutron-induced sequential transmutation of tungsten into rhenium and later on osmium is predicted to place the alloy composition close to the 100% phase field of brittle σ precipitates [16-18]. Therefore, it is of paramount importance to design the alloy composition and microstructure so as to enhance its ductility, and therefore to extend the temperature window of W-based alloys for safe reactor operation.

One promising route to increase ductility is to alloy tungsten with tantalum (Ta), since the latter also improves corrosion resistance [19] and its neutronic performance is relatively similar to that of tungsten [6, 16, 20, 21]. Ta also delays the compositional shift into the σ phase field [16]. However, the existing knowledge about the behaviour of W-Ta alloys in fusion-relevant radiation environments remains limited. Therefore, it is not yet possible to predict reliably the lifetime performance of the W-Ta material and its potential failure in reactor operation conditions. Past results about W doped with 5wt.% of Ta and subjected to 2 MeV W^+ ion irradiation at 300°C revealed a radiation-induced hardness increase at

relatively low damage levels, e.g. from 7.3 GPa in the unimplanted condition to 8.8 GPa at 0.07 dpa, attaining a saturation in hardness at 13 dpa [22]. Microstructural analysis showed that the loop number density in W-Ta alloys is greater than in W at the same damage level, but the average loop size is reduced [23]. Furthermore, implantation of 3000 appm helium in W-Ta alloys at 300°C induces a hardening effect larger than in the case of self-ion implantation [24]. In addition, a rapid increase in hardness was observed after 800MeV proton irradiation of tungsten up to a damage level of 0.8 dpa, followed by a lower rate of hardness increase at higher damage levels up to 23 dpa [25]. Despite these results, the mechanistic understanding of the structural damage formation and evolution in W-Ta alloys leading to the observed hardness increase is very fragmented and requires additional experimental evidence.

A suitable approach to monitor the formation and evolution of radiation-induced lattice defects in metallic materials is to perform in-situ experiments using a transmission electron microscope (TEM) coupled to an ion accelerator [26, 27]. However, the acceleration voltage in the electron gun of the microscope is normally not high enough to study regions in the TEM foil thicker than ~50-200nm. This implies that potential lattice defects, such as dislocation loops induced by radiation, could migrate to the sample surface, due to image forces, that would act as an effective defect sink. The consequence is a potential underestimation of the produced defect density, and/or changes in the morphology and predominant nature of the lattice defects [28, 29]. Radiation-induced dislocation loops were reported to migrate to the sample free surface in both single crystal and polycrystalline tungsten material, during an in-situ TEM experiment using proton energies between 0.5-8 keV in the temperature range of 20–800°C [30].

This study is devoted to the in-situ observation of radiation-induced lattice defects in W-5Ta alloy at 350^{o}C, and how they evolve with an increasing damage level at that

temperature. The potential impact of the free surface in the in-situ proton-irradiated samples was assessed by performing equivalent irradiations using a higher proton beam energy and analysing the lattice damage ex-situ using TEM. Additional irradiation experiments using equivalent conditions were performed on tungsten, and the results used as a base line to understand the effect of tantalum on the evolution of the structural damage induced by proton irradiation.

2. Experimental

The W-5wt.%Ta (W-5Ta) alloy was produced by powder metallurgy and provided by Plansee AG. After delivery, the material was annealed for 1 h at 1000°C for degassing [31]. The starting W material was provided by Goodfellow Cambridge Ltd. in the form 1mm-thick sheet. Both as-received materials were initially annealed in vacuum at 1400°C for 2 hours for recrystallization. The average grain size, as derived from Electron Backscattered Diffraction maps, was ~1 μm (W-5Ta) and ~3μm (W), respectively. 3mm-diameter TEM discs of both materials were prepared by mechanical pre-thinning, followed by electropolishing at a temperature of ~ -5°C using a Struers Tenupol-5 unit and an electrolyte comprising an aqueous solution of 0.5 wt.% Na_2S for electropolishing W, or a mixture of 15vol.% sulphuric acid (95%) and 85vol.% methanol in the case of W-5Ta. In-situ proton irradiation experiments were performed at the Microscope and Ion Accelerator for Materials Investigations (MIAMI-1 facility) located at the University of Huddersfield [32]. The TEM discs were placed in a high-temperature Gatan 652 double-tilt specimen holder, and then mounted in a JEOL JEM-2000FX TEM operating at an accelerating voltage of 200 kV. The TEM is installed at the end of a beam line connected to an electrostatic accelerator that produces ion beams with energies up to 100 keV. The ion beam enters the microscope at 30^o with respect to the electron beam direction. We performed step-wise sample irradiations

using a 40 keV proton beam at a temperature of 350(2)°C. At the end of the experiment, we achieved a proton fluence of 9.5×10^{17} ions/cm^2 for W and 9.7×10^{17} ions/cm^2 for W-5Ta.

Additionally, we performed two independent ex-situ proton irradiation experiments, attaining a damage level of 1 and 2 dpa respectively at the Bragg peak position. In each of those experiments, we mounted both W and W-5Ta samples simultaneously. The samples were irradiated using a 3 MeV proton beam produced by a 5 MV tandem ion accelerator installed at the University of Manchester [33]. The two samples were kept at a temperature of 350(4)°C. The temperature uniformity was monitored during the experiment using an IR camera located at 30° with respect to the sample surface. In addition, thermocouples were spot welded on the samples outside the irradiated area. Liquid indium was used to improve the thermal contact between the samples and the NIMONIC75® alloy block of the sample stage. A summary of the irradiation conditions of the experiments performed at both irradiation facilities is shown in Table 1. We prepared TEM discs from the samples irradiated ex-situ to a fluence of 1.2×10^{19} protons/cm^2, using the electropolishing conditions described above. The damaged structures were characterised using an FEI Tecnai T20 Transmission Electron microscope with LaB_6 crystal, equipped with a double-tilt specimen holder and operating at 200kV. The determination of the Burgers vector $\boldsymbol{b}$ of the observed dislocations made use of the $\mathbf{g}.\mathbf{b}=0$ invisibility criterion, where $\boldsymbol{g}$ denotes the scattering vector. The foil thickness was derived from the fringes spacing of the convergent beam electron diffraction pattern, and was used to obtain the dislocation density at each selected radiation dose [34]. The interstitial or vacancy nature of the dislocation loops was assessed by applying the inside-outside contrast method [34]. The surface of the W and W-5Ta samples irradiated ex-situ was also characterised by secondary electron imaging using a FEI Quanta 250 FEG-SEM and an accelerating voltage of 20 kV. Furthermore, the damage profile was simulated using the SRIM software with the quick Kinchin–Pease approach. [35,36]. We used a value for the

displacement energy of 90 eV and default values for other software settings [37], together with the total charge deposited on the sample during the irradiation experiment. The simulated damage profiles for both in-situ and ex-situ experiments are displayed in Fig. 1, and the penetration depth from which TEM foils were prepared for ex-situ analysis is also indicated in this figure.

3. Results

The evolution of the structural damage in W-5Ta and W up to a damage level of 0.7 dpa at a temperature of 350(2)°C, as observed by in-situ TEM during proton irradiation, is shown in Fig. 2 and 3, respectively. In both materials dislocation loops are already visible at a damage level of 0.1 dpa, homogeneously distributed in the matrix, and their size appears to increase with radiation damage. The dependence of the average loop size and number density with radiation damage level for both materials is shown in Fig. 4. The average loop length and width in both W-5Ta and W increases progressively up to a damage level of 0.3 dpa. At higher damage levels, the average loop width in both materials reaches saturation, with a somewhat higher value for W (29(7) nm) than for W-5Ta (21(4) nm) at 0.7 dpa. Moreover, the loop length in W-Ta also saturates beyond 0.3 dpa, at a value of 33(10) nm. However, the loop length in the case of W continues to increase, and does not reach saturation at 0.7 dpa, where its loop length takes a value of 183(50) nm. The increase in loop length in W with damage level occurs simultaneously with a continuous decrease in the loop number density. This deviates from the behaviour observed in W-5Ta, where the number density of the loops also seems to gradually level off and saturate at damage levels higher than 0.3 dpa. At the highest damage level of 0.7 dpa in this study, the number density takes a value of 2.1×10^{21} m^{-3} (W-5Ta) and 0.8×10^{21} m^{-3} (W), respectively. Post-morten TEM analysis of both in-situ irradiated materials up to 0.7dpa showed that the loops are of interstitial nature and with Burgers vector of a/2 <111>.

Bright field TEM images of W and W-5Ta samples irradiated ex-situ and in-situ at selected damage levels are shown for comparison in Fig. 5. Ex-situ TEM samples show the presence of dislocation tangles, together with a number of dislocation loops similar to those observed in the in-situ inspected samples. The coexistence of dislocation loops and tangles is especially noticeable in the ex-situ W sample at a damage level of 0.3 dpa. Fig. 6 displays the secondary electron images of both materials irradiated ex-situ up to two different damage levels at the Bragg peak position, namely 1 and 2 dpa. The surface of W presents a significant number of blisters, whose size increases with damage level. This is in stark contrast with the surface characteristics observed for the W-5Ta alloy, where both the number and size of blisters are significantly reduced as compared to those observed in W at the same damage level. In fact, in W-5Ta blisters start to be visible at the damage level of 2 dpa at the Bragg peak position, whereas in the case of W the blisters are already formed and grown to a few hundreds of microns in size at this damage level.

4. Discussion

Molecular dynamic simulations have revealed that the damaged structure in bcc metals is initially characterized by a relatively large fraction of individual vacancy and self-interstitial atom (SIA) defects, together with a number of small mobile SIAs clusters [38]. The most stable interstitial cluster configuration in W is predicted to be $a/2$ <111> dislocation loops [39] and this coincides with our TEM results for both W and W-5Ta alloys. However, vacancy dislocation loops are metastable with respect to the transformation into spherical voids [39], and were not observed in the W and W-5Ta samples proton irradiated at 350°C. The vacancy migration enthalpy in tungsten is reported to take the value of 1.78 eV [40,41]. In fact, the irradiation temperature of 350°C is below the critical temperature of 470°C for the recovery in W due to long-range vacancy migration [41]. Therefore, the radiation damage evolution in this study is mainly governed by the nucleation, diffusion and growth of

a/2 <111> interstitial dislocation loops. The average loop size in both materials increases, whereas the number density reduces, with the damage level up to 0.3 dpa. Beyond this level, the loop length in W continues to increases, but the loop width gradually levels off. This trend gives rise to the appearance of the dislocation loop strings in W at higher damage level. Such evolution of the microstructure is in contrast with the loop behaviour in W-5Ta at higher damage levels, where both the loop width and length saturate. The formation of the elongated loops and their ordering in strings could be explained by their mutual elastic interaction and minization of the dislocation strain energy. The fact that the same process is not observed in W-Ta suggests that Ta might have an impact on the mobility of dislocation loops (and single SIAs).

The free surface of the sample is expected to act as an effective non-biased sink for all mobile defects. However, the 1D migration of SIAs, attaining <111> crowdion configuration, should lead to their preferred capture at the surface, thus generating a super-saturation of vacancies. Consequently, 3D-migrating vacancies may form clusters in the near-surface regions of the sample [42]. In this study, we have not observed the appearance of vacancy clusters in the thin foil samples irradiated in-situ. The presence of a relatively high dislocation density, as observed in both the W and W-5Ta samples, would impose high cross section for the SIA-loop interaction and minimise the surface effect [43]. Furthermore, the stress field around dislocation loops is altered in the vicinity of the free surface, so that an attractive image force is generated that would drive the dislocation loops towards the surface. The image force is in competition with the glide and climb forces, that depend on the loop spacing and size, respectively [44]. Our ex-situ TEM analysis reveals the coexistence of dislocation tangles and loops in both materials, as opposed to the lack of dislocation tangles in the in-situ specimens, see Fig. 5. This difference points out to the microstructure observed ex-situ by TEM as corresponding to a later stage in the radiation damage accumulation, as

compared to the in-situ samples where a fraction of dislocation loops may have escaped to the free surface of the sample. However, we have observed neither changes in the nature of the dislocation loops and their Burgers vector, nor the presence of a significant number of vacancy clusters [29].

The string-like features or dislocation strings observed in W samples irradiated in-situ at damage levels above 0.3 dpa resemble rafting observed on (11-1) and (111) planes in neutron-irradiated W samples up to a fluence of ~1 $\times 10^{22}$ n cm^{-2}, assuming a Burgers vector of the loops to be $a/2$ <111> [45]. A density of rafts was estimated as 6.1×10^{14} rafts cm^{-2} at 430°C, and the rafts were likely to be associated with dislocation lines. The rafts, and most likely the string-like features observed in the proton-irradiated W samples in this study, may result from two simultaneously operating mechanisms: (1) the preferential drift of SIAs to dislocations loops and (2) the glide and self-climb of those loops.

The addition of Ta seems to hinder the occurrence of string-like features and subsequently also of presence of the blisters. The thermal vacancy-mediated diffusion of Ta in W is relative slow, with an activation energy of E^a = 6.20eV and a pre-exponential factor of $D_0 = 6.20 \times 10^{-4}$ m^2/s [21]. An Arrhenius-type dependence of the diffusion coefficient (D) on temperature (T) yields a value of $D = 4.3 \times 10^{-54}$ m^2/s at a temperature of 350°C. In fact, Ta segregation and clustering has not been observed in W-4.5Ta(at.%) under 2MeV W^+ irradiation at 300 and 500°C up to a damage level of 33 dpa [21]. However, recent Density Functional Theory calculations revealed the strong repulsive interaction between Ta and interstitial clusters such as crowdion [46] or dumbbell [47] configurations. The presence of Ta retards the mobility of SIAs and interstitial dislocation loops, and consequently the loop growth and coalescence [23], eventually transiting into dislocation strings.

Once implanted, H is expected either to diffuse back to the surface or deeper into the W or W-5Ta sample [48], preferentially via a TIS-TIS diffusion pathway, where 'TIS'

denotes a tetrahedral interstitial site in the bcc lattice of W [49]. The diffusion coefficient of H in bulk W is reported to take the form $D = 4.1\times10^{-7}\times\exp(-0.39\ \text{eV}/kT)$, assuming that trapping effects are negligible [50, 51]. In fact, the energy barrier for outward diffusion of H from the first subsurface sites is predicted to be small, namely ≤0.06 eV [52], and the actual H concentration in bulk W at 327°C is only 2.3×10^{-10}, in units of the atomic fraction of H (H/W) [53]. However, H can become trapped at lattice defects or impurities [54]. We have observed the formation of dislocation loops under proton irradiation, and their evolution in W into dislocation tangles and strings. At a later stage those dislocation structures can induce H trapping and accumulation in sub–surface regions of the W and W-5Ta samples. Both radiation-induced dislocation loops and dislocations formed by cold work are reported to act as effective traps for implanted deuterium in W [55]. As a consequence, a H saturated layer in the near surface region of the sample is formed, whose thickness increases continuously with proton fluence. The oversaturated H forms bubbles [54], with an internal gas pressure of the order of GPa as derived from Finite Element Model calculations [56]. We have detected a significant number of dome-like blisters on the surface of the ex-situ proton-irradiated W samples, whose size increases with damage level, see Fig. 6. However, the saturation of blisters or surface exfoliation was not observed at the highest damage level of this study. In contrast to the evolution of blisters observed in W, the ex-situ W-5Ta samples reveal a reduced blistering phenomenon, and blisters start to be visible only at a damage level of 2 dpa (at the Bragg peak position), see Fig. 6. Ta atoms are not expected to segregate in ion irradiated samples at those damage levels [21], and would not act as effective trapping sites for H, as compared to the role of radiation-induced dislocations. Therefore, the role of Ta which delays the appearance of the TEM-visible lattice damage, seems to also hinder the occurrence of blistering in W. Doping with Ta could therefore restrict the H-induced blister

phenomenon, and the resultant inventory of H isotopes, expected in W under tokamak edge plasma conditions involving neutron irradiation damage [57].

5. Conclusions

The combined approach to irradiate W and W-5Ta samples using independently proton beams of two different energies, i.e. 40keV and 3MeV, coupled with transmission electron microscopy to assess in-situ/ex-situ the radiation induced damage, allows one to probe the defect structure evolution in these materials at different stages in the damage process. In both materials, $a/2$ <111> interstitial dislocation loops form under proton irradiation. The loop size increases whereas the loop density reduces with increasing damage levels up to 0.3 dpa. Loop saturation takes place in W-5Ta at higher damage levels than in W. In contrast, the loop length in W continues to increase with damage level and gives rise to the formation of dislocation strings. Later stages in the damage accumulation sequence are characterised by the co-existence of dislocation loops and networks in both materials. The evolution of dislocation loops into strings and networks leads to significant hydrogen trapping and the occurrence of surface blisters. Ta solid solution delays the evolution of the dislocation structures with increasing proton-induced damage level, as compared to non-doped W, and consequently reduces the formation of hydrogen bubbles and the resultant surface blisters.

Acknowledgements

The work described was supported by the Dalton Cumbrian Facility Project, a joint facility of The University of Manchester and the Nuclear Decommissioning Authority. We thank A.D. Smith and N. Mason for their assistance during the proton irradiation experiment. We acknowledge the support of EPSRC for the development of the MIAMI-1 Facility (EP/E017266/1).

References

[1] M. Merola, F. Escourbia, R. Raffray, P. Chappuis, T. Hirai, A. Martin, Fusion Eng. Des. 89 (2014) 890.

[2] J.H. You, Nucl. Fusion 55 (2015) 113026.

[3] D.M. Yao, G.N. Luo, Z.B. Zhou, L. Cao, Q. Li, W.J. Wang, et al., Phys. Scr. T167 (2016) 014003.

[4] E. Lassner, W. S. Schubert, Tungsten: Properties, Chemistry, Technology of the Element, Alloys and Chemical Compounds, 1999, Springer, New York, NY.

[5] D.M. Duffy, Phil. Trans. R. Soc. A 2010 368, 3315.

[6] M. Rieth, S.L. Dudarev, S.M. Gonzalez de Vicente, J. Aktaa, T. Ahlgren, S. Antusch, et al., J. Nucl. Mater. 432 (2013) 482.

[7] R.G. Abernethy, Mater. Sci. Technol. 33 (2017) 388.

[8] L. Giancarli, J.P. Bonal, A. Li Puma, B. Michel, P. Sardain, J. F. Salavy, Fusion Eng. Des. 75–79 (2005) 383.

[9] N. Baluc, Phys. Scr. T138 (2009) 014004.

[10] B. Bazyleva, G. Janeschitz, I. Landman, S. Pestchanyi, A. Loarte, G. Federici, et al., Fusion Eng. Des. 83 (2008) 1077.

[11] T. Shen, Y. Dai, Y. Lee, J. Nucl. Mater. 468 (2016) 348.

[12] V. Philipps, J. Nucl. Mater. 415 (2011) 52.

[13] H. Bolt, V. Barabash, G. Federici, J. Linke, A. Loarte, J. Roth, K. Sato, J. Nucl. Mater. 307-311 (2002) 43.

[14] S.J. Zinkle, N. M. Ghoniem, Fusion Eng. Des. 51–52 (2000) 55.

[15] Ph. Mertens, V. Thompson, G.F. Matthews, D. Nicolai, G. Pintsuk, V. Riccardo, et al., J. Nucl. Mater. 438 (2013) S401.

[16] G.A. Cottrell, J. Nucl. Mater. 334 (2004) 166.

[17] T. Tanno, A. Hasegawa, J.-C. He, M. Fujiwara, S. Nogami, M. Satou, T. Shishido, K. Abe, Mater. Trans. 48 (2007) 2399.

[18] M. R. Gilbert, J.-C. Sublet, Nucl. Fusion, 51 (2011) 043005.

[19] T.E. Tietz, J.W. Wilson, Behavior and Properties of Refractory Metals, Stanford University Press, 1965.

[20] D. Jiang, Q. Wang, W. Hu, Z. Wei, J. Tong, H. Wan, J. Mater. Res. 31 (2016) 3401.

[21] A. Xu, D.E.J. Armstrong, C. Beck, M.P. Moody, G.D.W. Smith, P.A.J. Bagot, et al., Acta Mater. 124 (2017) 71.

[22] D. E. J. Armstrong, A. J. Wilkinson, S. G. Roberts, Phys. Scripta, T145 (2011) 014076.

[23] X. Yi, M. L. Jenkins, K. Hattar, P. D. Edmondson, S. G. Roberts, Acta Mater. 92 (2015) 163.

[24] C.E. Beck, S.G. Roberts, P.D. Edmondson, D.E.J. Armstrong, MRS Proc. 1514 (2013) 99.

[25] S.A. Maloy, M.R. James, W. Sommer, G.J. Willcutt, M. Lopez, T.J. Romero, Mater. Trans. 43 (2002) 633.

[26] J.A. Hinks, Nucl. Instr. Meth. Phys. Res. A 267 (2009) 3652.

[27] S. Ishino, Mater. Trans. 55 (2014) 396.

[28] T. Muroga, N. Yoshida, N. Tsukuda, K. Kitajima, M. Eguchi, Mater. Sci. Forum 15-18 (1987) 1087.

[29] A. Prokhodtseva, B. Décamps, R. Schäublin, J. Nucl. Mater. 442 (2013) S786.

[30] R. Sakamoto, T. Muroga, and N. Yoshida, J. Nucl. Mater. 222 (1995) 819.

[31] Y. Zayachuk, M.H.J. 't Hoen, P.A. Zeijlmans van Emmichoven, D. Terentyev, I. Uytdenhouwen, G. van Oost, Nucl. Fusion 53 (2013) 013013

[32] J.A. Hinks, J.A. van den Berg, S.E. Donnelly, J. Vac. Sci. Technol. A 29 (2011) 21003.

[33] P.T. Wady, A. Draude, S.M. Shubeita, A.D. Smith, N. Mason, S.M. Pimblott, E. Jimenez-Melero, Nucl. Instr. Meth. Phys. Res. A 806 (2016) 109.

[34] M.L. Jenkins, M.A. Kirk, Characterization of Radiation Damage by Transmission Electron Microscopy, IOP Publishing Ltd, 2001.

[35] J.F. Ziegler, J. Appl. Phys. 85 (1999) 1249.

[36] J.F. Ziegler, M.D. Ziegler, J.P. Biersack, Nucl. Instr. Meth. Phys. Res. B 268 (2010) 1818.

[37] ASTM E521-96, Standard Practice for Neutron Radiation Damage Simulation by Charged-particle Irradiation, 2009.

[38] B.N. Singh, J.H. Evans, J. Nucl. Mater. 226 (1995) 277.

[39] M.R. Gilbert, S.L. Dudarev, P.M. Derlet, D.G. Pettifor, J. Phys.: Condens. Matter 20 (2008) 345214.

[40] D. Nguyen-Manh, A. P. Horsfield, S. L. Dudarev, Phys Rev. B 73 (2006) 020101.

[41] D.N. Seidman, Scripta Metall. 13 (1979) 251.

[42] M. Kiritani, Mater. Sci. Forum 15-18 (1987) 1023.

[43] D.I.R. Norris, Radiat. Eff. 15 (1972) 1.

[44] F. Ferroni, E. Tarleton, S. Fitzgerald, Modelling Simul. Mater. Sci. Eng. 22 (2014) 045009.

[45] V.K. Sikka, J. Moteff, J. Nucl. Mater. 46 (1973) 217.

[46] M. Muzyk, D. Nguyen-Manh, K. J. Kurzydłowski, N. L. Baluc, S. L. Dudarev, Phys. Rev. B 84 (2011) 104115.

[47] W. Setyawan, G. Nandipati, R.J. Kurtz, J. Nucl. Mater. 484 (2017) 30.

[48] R.A. Causey, J. Nucl. Mater. 300 (2002) 91.

[49] G.-H. Lu, H.-B. Zhou, C.S. Becquart, Nucl. Fusion 54 (2014) 086001.

[50] R. Frauenfelder, J. Vac. Sci. Technol. 6 (1969) 388.

[51] K. Heinola, T. Ahlgren, J. Appl. Phys. 107 (2010) 113531.

[52] D.F. Johnson, E.A. Carter, J. Mater. Res. 25 (2010) 315.

[53] Y.-L. Liu, H.-B. Zhou, Y. Zhang, J. Alloys Comp. 509 (2010) 8277.

[54] T. Tanabe, Phys. Scr. T159 (2014) 014044.

[55] R. Sakamoto, T. Muroga, N. Yoshida, J. Nucl. Mater. 2.3-237 (1996) 776.

[56] N. Enomoto, S. Muto, T. Tanabe, J.W. Davis, A.A. Haasz, J. Nucl. Mater. 385 (2009) 606.

[57] Y. Ueda, J.W. Coenen, G. De Temmerman, R.P. Doerner, J. Linke,V. Philipps, et al., Fusion Eng. Des. 89 (2014) 901.

Tables

Table 1. Main parameters used during the proton irradiation of W and W-Ta samples. The damage level of the in-situ samples corresponds to the average value over the disc thickness of ~100 nm studied by TEM (see inset of Fig.1). In this case, the samples were studied in-situ by TEM at selected incremental damage levels up to 0.7 dpa. The fluence given in the table refers to the total value achieved at the end of the in-situ irradiation experiment, corresponding to the damage level of 0.7 dpa. In contrast, the damage levels mentioned for the ex-situ irradiation corresponds to the value from where the foils where extracted for TEM analysis, using the samples irradiated to a fluence of 1.2×10^{19} protons/cm^2. The damage is spread along a larger depth in the ex-situ 3 MeV irradiation, as compared to the higher slope seen in the damage profile from the in situ 40 keV irradiation (see Fig. 2).

	In-situ		***Ex-situ***	
Material	**W**	**W-5Ta**	**W**	**W-5Ta**
Temperature (°C)	350±2		350±4	
Proton energy	40 keV		3 MeV	
Current (nA)	0.5	0.45	12 000	
Fluence (ions/cm^2)	9.5×10^{17}	9.7×10^{17}	1.2×10^{19}	
Flux (ions/cm^2/s)	2.4×10^{14}	2.2×10^{14}	4.8×10^{17}	
Damage rate (dpa/s)	~1 $\times10^{-4}$		~3.5×10^{-6}	~4.6×10^{-6}
Damage level (dpa)	0.7		0.3	0.4

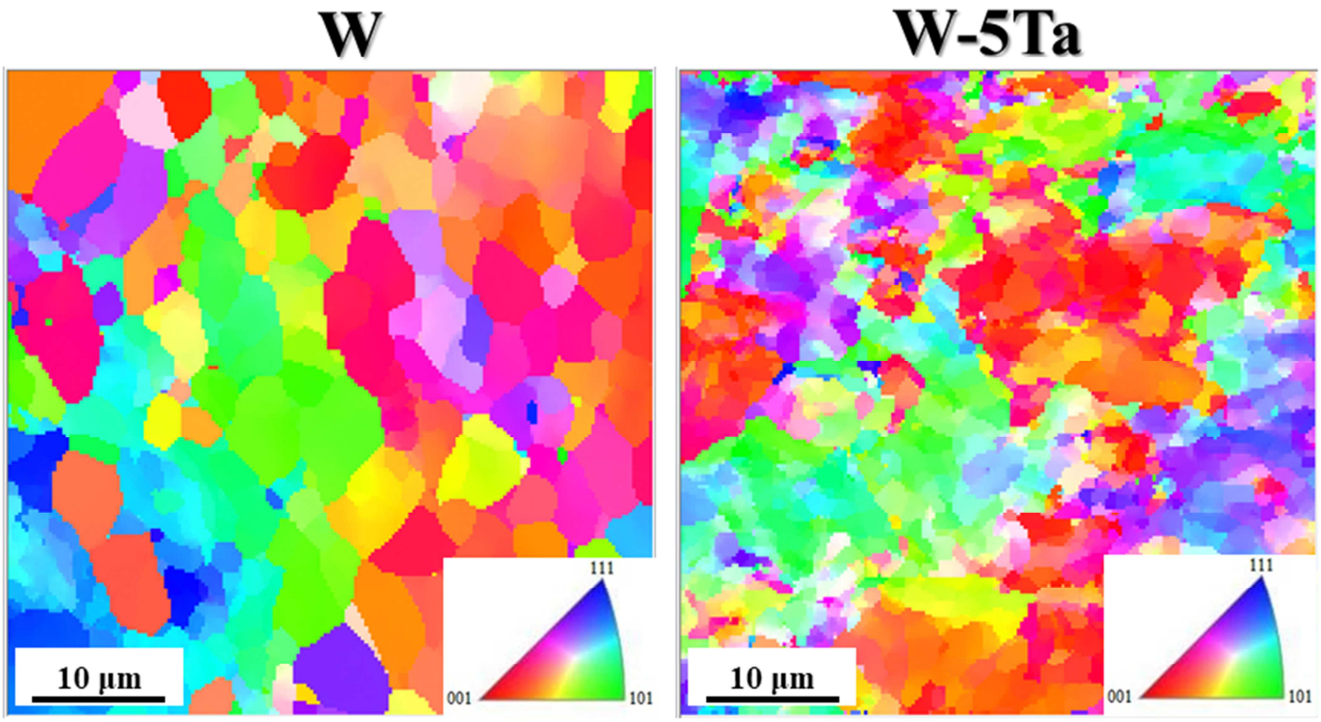

Fig. 1

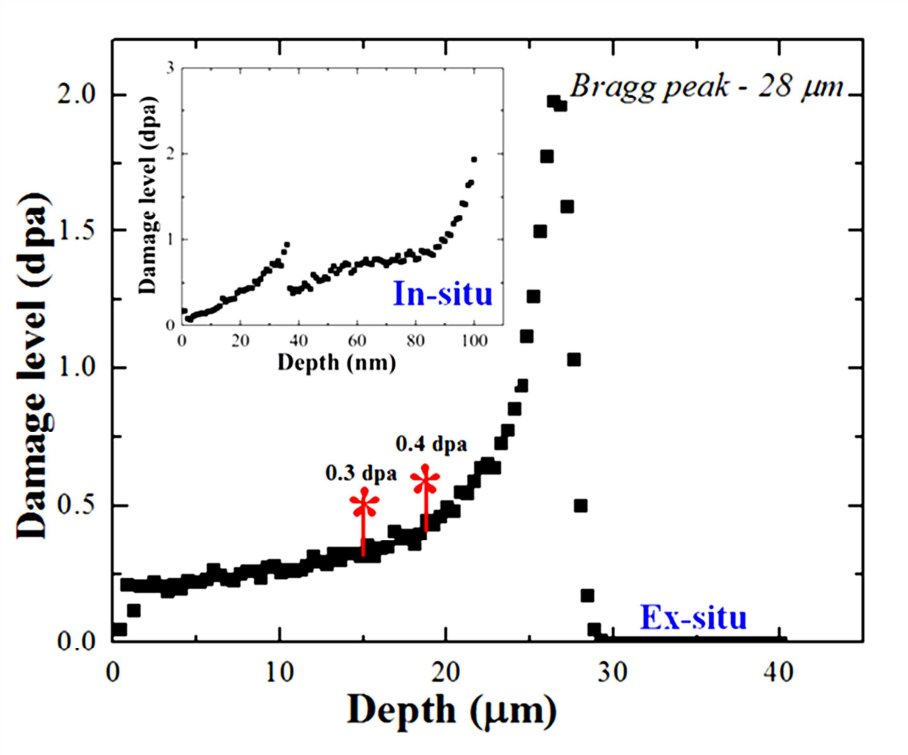

Fig. 2

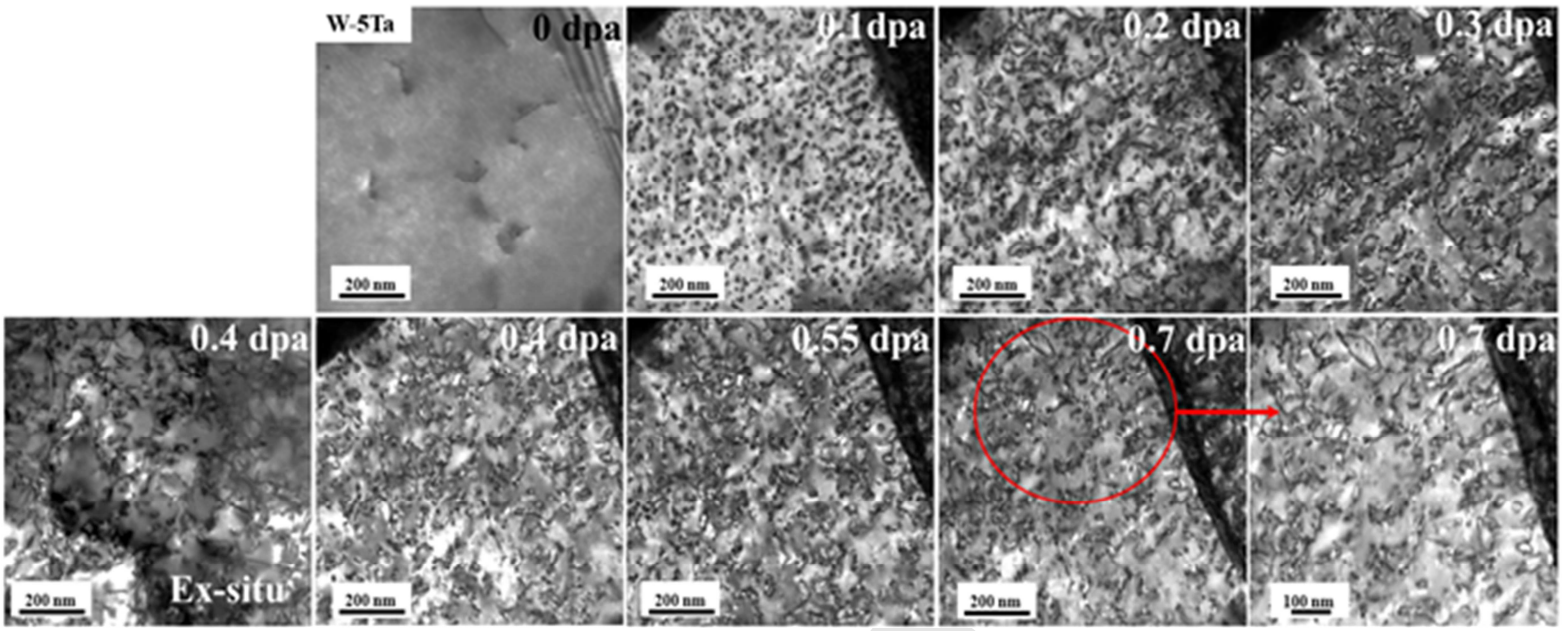

Fig. 3

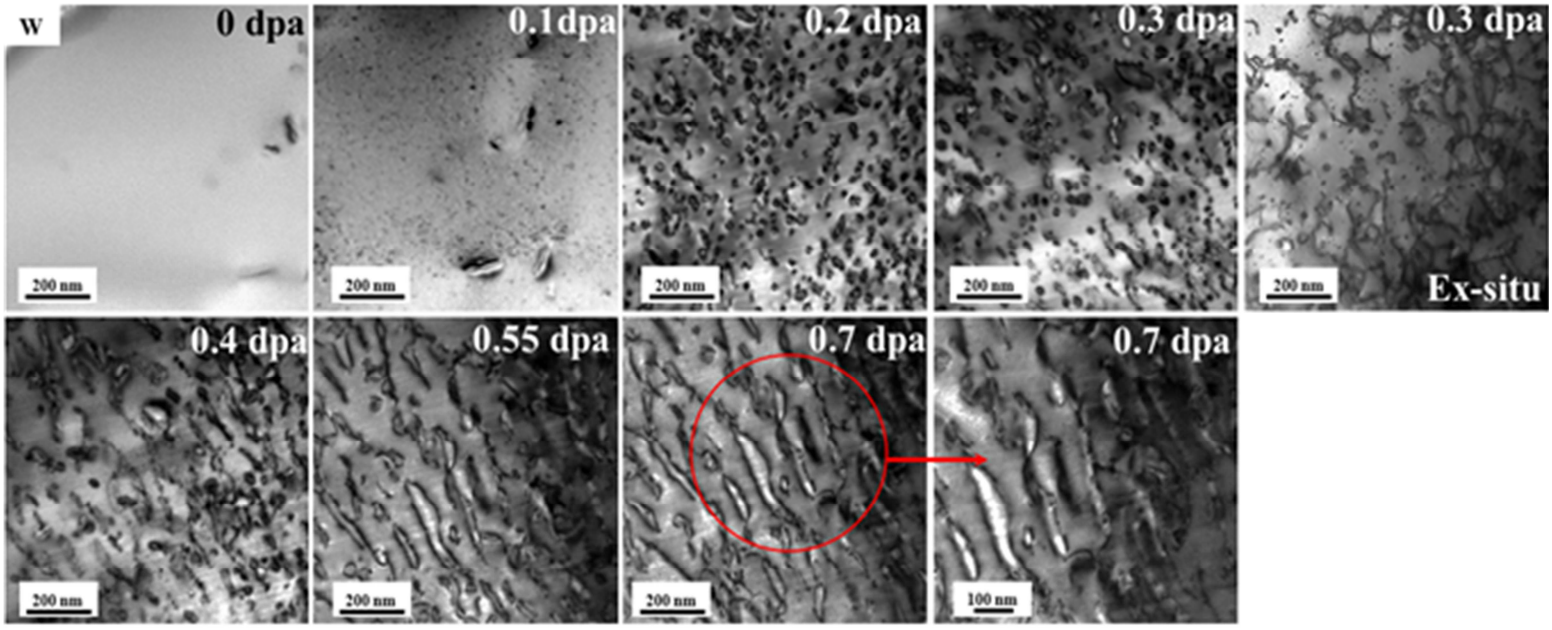

Fig. 4

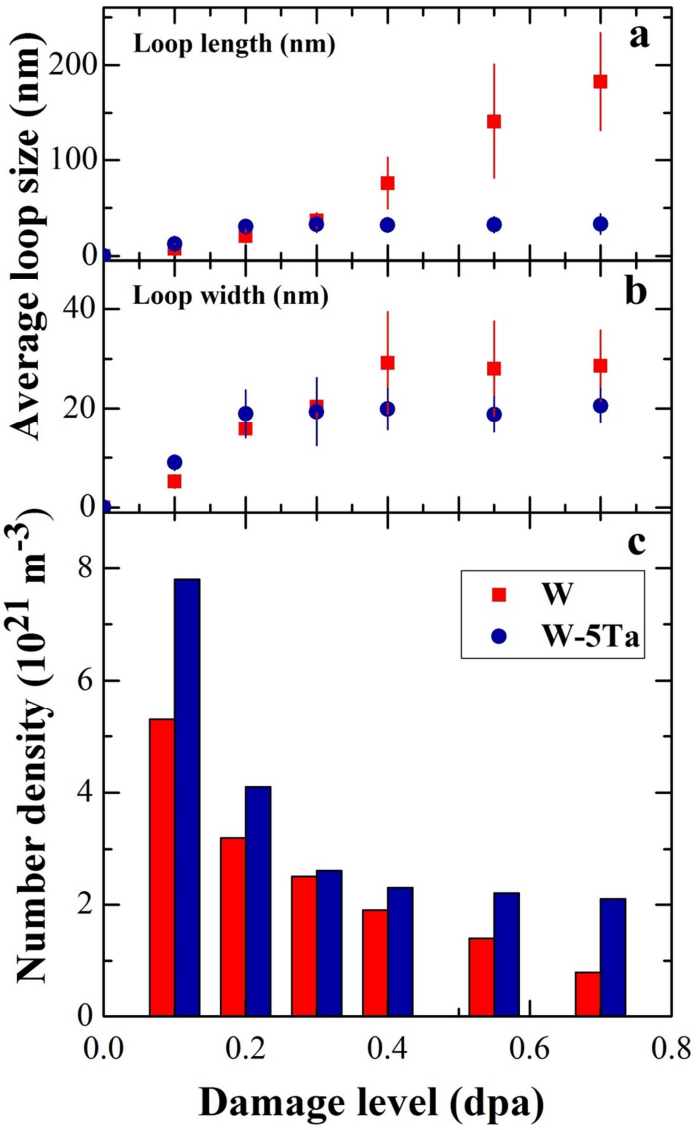

Fig. 5

Highlights

1. Interstitial *a*/2 <111> loops form in proton-irradiated W and W-5Ta at 350°C
2. At 0.3dpa loop length in W-5Ta reaches saturation, whereas it still increases in W
3. Dislocation loops in W evolve into dislocation strings above 0.3dpa
4. At high damage levels dislocation loops and tangles coexist in both W and W-5Ta